

A CoGeNT Modulation Analysis

Patrick J. Fox^a, Joachim Kopp^a, Mariangela Lisanti^b, Neal Weiner^{c,d}

^a *Theoretical Physics Department, Fermi National Accelerator Laboratory, Batavia, Illinois, USA*

^b *PCTS, Princeton University, Princeton, NJ 08540*

^c *Center for Cosmology and Particle Physics, Department of Physics, New York University, New York, NY*

^d *School of Natural Sciences, Institute for Advanced Study, Einstein Drive, Princeton, NJ 08540*

ABSTRACT: We analyze the recently released CoGeNT data with a focus on their time-dependent properties. Using various statistical techniques, we confirm the presence of modulation in the data, and find a significant component at high ($E_{ee} \gtrsim 1.5$ keVee) energies. We find that standard elastic WIMPs in a Maxwellian halo do not provide a good description of the modulation. We consider the possibility of non-standard halos, using halo independent techniques, and find a good agreement with the DAMA modulation for $Q_{Na} \approx 0.3$, but disfavoring interpretations with $Q_{Na} = 0.5$. The same techniques indicate that CDMS-Ge should see an $O(1)$ modulation, and XENON100 should have seen 10-30 events (based upon the modulation in the 1.5-3.1 keVee range), unless \mathcal{L}_{eff} is smaller than recent measurements. Models such as inelastic dark matter provide a good fit to the modulation, but not the spectrum. We note that tensions with XENON could be alleviated in such models if the peak is dominantly in April, when XENON data are not available due to noise.

KEYWORDS: .

1. Introduction

The CoGeNT Collaboration has recently published results from the first fifteen months of data taking [1, 2]. Since their first data release more than a year ago, they continue to observe an unexplained excess in the spectrum of nuclear recoil scattering rate and now claim an annual modulation of 2.8σ . This preliminary evidence for a modulation is an important step towards determining the nature of CoGeNT’s unexplained spectrum and has been claimed to be evidence for a ~ 7 GeV dark matter [2, 3]. In this work, we present a comprehensive statistical analysis of the CoGeNT data and show that the modulation spectrum is hard to achieve with a conventional light elastic WIMP in a standard Maxwellian halo.

Direct detection experiments such as CoGeNT search for the scattering of dark matter off nuclei in ground-based detectors. The spectrum of nuclear recoil energies depends on the mass and scattering cross section of the dark matter, as well as its velocity distribution in the Galaxy. One of the most distinctive features of a dark matter signal is that it should modulate annually due to the motion of the Earth’s rotation about the sun [4]. In particular, the flux of dark matter as observed in the lab frame is larger in the summer, when the Earth is moving in the same direction as the Sun, than in the winter, when the Earth’s motion is against that of the Sun [5].

Observing an annual modulation in a potential signal is a crucial step in confirming its origin as dark matter. Direct detection experiments face the challenge of distinguishing dark matter nuclear recoils from a list of potential backgrounds. In most cases, experiments utilize a combination of ionization, scintillation, or heat to separate out nuclear recoils [6]. But the possibility of contamination in the nuclear recoil band remains, for instance due to unaccounted for radioactive decays. If the signal in the nuclear recoil band modulates with the period and phase expected for a dark matter signal, however, it would be a strong indication of the nature of the interaction producing the signal.

To date, only the DAMA [7, 8] and CoGeNT [1, 2] experiments have claimed an annual modulation signal. The DAMA experiment, which uses target crystals of NaI(Tl), claims an 8.9σ modulation with period 0.999 ± 0.002 years and peaking at 146 ± 7 days. The CoGeNT experiment, which uses a Ge target, has recently claimed an annual modulation signal with their first fifteen months of data. They have shown that, in an energy bin ranging from 0.5-3.0 keVee¹, they observe a maximal modulation with best-fit modulation fraction of $16.6 \pm 3.8\%$, period 347 ± 29 days, and minimum at Oct. 16 ± 12 days. In this energy range, the significance is 2.8σ . When the CoGeNT data are fit with a dark matter signal, constant and exponential background, it is consistent with a dark matter mass of roughly 7-8 GeV and $\sigma \sim 10^{-4}$ pb, which falls very close to the region of parameter space that is consistent with DAMA [1, 3].

¹The notation keVee refers to the “electron equivalent energy in keV”, which is defined as the reconstructed recoil energy under the assumption that it is carried by an electron. For nuclear recoils, only part of the recoil energy is visible in the detector—an effect which has to be corrected for by dividing the visible energy by a quenching factor—so that the energy threshold for nuclear recoils is higher than that for electron recoils. When referring to a nuclear recoil energy, we will use the notation “keVnr”.

The light dark matter interpretation of CoGeNT and DAMA has been challenged by null results from other direct detection experiments, such as Xenon100 [9], Xenon10 [10, 11], Simple [12, 13], and CDMS [14, 15]. The compatibility of the Xenon and CoGeNT results have been discussed in greater detail in [16, 17, 18, 19, 20]. Reconciling the CDMS and CoGeNT results is more challenging since the two use the same target material and CDMS has reported an event rate significantly below that of CoGeNT in the same energy range; however, it has been claimed that errors in the energy calibration can potentially cause the discrepancy [21]. As we shall see, our conclusions on the modulation at CoGeNT will not be strongly dependent on these details.

In this work, we present a detailed statistical analysis of the CoGeNT results using the publicly available data [22], going beyond the recently presented analyses [23, 24] which use only the 2 bin data shown in [2]. We first introduce the statistical tools we use in Sec. 2 and then, in Sec. 3, perform a model-independent analysis of the modulated and unmodulated rate, period, and phase in a range of energies. We show that the modulation is most significant in the energy region between 1.5–3.0 keVee, even though the best fit modulation amplitude is larger at low energies (0.5–0.9 keVee), but with a large error bar. In the region of greatest significance, the period of the modulation is approximately one year and the phase is $t_0 \sim 106$ days, although neither the period nor the phase can be well-constrained in energy regions with lower significance. In Sec. 4, we discuss the implications of these results for dark matter and present spectra of the modulation amplitude for cases with and without additional background components. We also show how the hypothesis of a light, elastically scattering WIMP (weakly interacting massive particle), is strained by the fact that most of the modulation occurs at larger energies. We use techniques to compare to other experiments independent of the halo model and find that for spin-independent scattering both CDMS-Ge and CDMS-Si indicate that whatever signal is present at high energies should be $\sim 100\%$ modulated. The significant modulation at energies above 1.5 keVee would predict large rates at XENON100 unless the L_{eff} is smaller than recent measurements. At the same time, we find that such a mapping gives remarkable agreement between the rates of modulation at CoGeNT and DAMA, while disfavoring earlier approaches with large Q_{Na} .

2. CoGeNT Data and Analysis Techniques

We perform our analysis using the data available from the CoGeNT collaboration upon request [22]. The run spans 458 days, starting on December 4, 2009, of which 442 days were live. The known background in the energy region of interest arises from cosmogenic L-shell electron capture events. We detail how we account for these backgrounds, $f_{\text{peaks}}(E)$, the efficiency, $f_{\text{eff}}(E)$, and the deadtime, described by $f_{\text{gaps}}(E)$, of the experiment in Appendix A.

A binned chi-squared analysis of the data has been used to show that there is a 2.8σ significance for modulation in the 0.5-3.0 keVee energy bin [2, 3]. In addition to a similar binned chi-squared analyses, we will introduce two alternative statistical tests that are appropriate for searches of periodicities in data: the unbinned maximum likelihood method [25] and the

Lomb-Scargle periodogram [26, 27]. Both these tests have been used, for example, in searches for periodicities in the solar neutrino flux from the Sudbury Neutrino Observatory [28]. Since here we are most interested in studying the time variation of the data, and we wish to remain agnostic to the distribution of events in energy, we will bin the events in energy but not in time. Later, when investigating the possibility of whether or not the data are explained by dark matter (DM), we will carry out fully binned and fully unbinned analyses, see Section 4. Below, we review these statistical tests and then show the results of the analyses in studies on the period, phase, modulation, and significance of the data in the following sections. We note that where the different techniques can be compared they give qualitatively similar results.

2.1 Binned Analysis

In the binned analysis we carry out a simple chi-squared analysis on events in a given energy range, binned in time. The events, at energies E_i , are reweighted by f_{eff}^{-1} , and then the known cosmogenic background in each bin is subtracted. Also, a correction is applied to those time bins overlapping with the shutdown periods of the detector. The errors in each bin are treated as Gaussian², based on the original bin contents before reweighting or subtraction. The subtracted binned data are then fit with a modulated spectrum of the form

$$R(t) = A_0(1 + A_1 \cos(\omega(t - t_0))) , \quad (2.1)$$

where A_0 is the unmodulated rate which may contain contributions from both a DM component and any constant backgrounds, A_1 is the modulation fraction, ω is the oscillation period and t_0 is the phase, all times are taken relative to January 1st, 2010. We consider fits where all the parameters are allowed to float as well as restrictions, where the frequency is fixed to $\omega_0 = 2\pi/\text{year}$, where the frequency is fixed to ω_0 and the phase is fixed to that expected from DM in the standard halo model (SHM), $t_0 = 152$ days, and the null hypothesis, $A_1 = 0$.

2.2 Unbinned Analysis

To maintain access to all the information contained in the time distribution of events we carry out an unbinned maximum likelihood analysis. We use this method to test the hypothesis that, in any given energy range, the excess data above backgrounds follow a rate distribution of the form $A_0(1 + A_1 \cos(\omega(t - t_0)))$. To do so we consider events in the energy range $(E_{\text{low}}, E_{\text{high}} = E_{\text{low}} + \Delta E)$, and take as their probability density function (PDF),

$$\begin{aligned} \phi(t) = & \left[0.33 \text{ kg} \times \Delta E \bar{f}_{\text{eff}}(E) \left(A_0(1 + A_1 \cos(\omega(t - t_0))) \right) \right. \\ & \left. + \int_{E_{\text{low}}}^{E_{\text{high}}} f_{\text{cosmo}}(E, t) f_{\text{eff}}(E) \right] f_{\text{gaps}}(t) , \end{aligned} \quad (2.2)$$

²Unless very narrow energy bins are considered this is a reasonable approximation for the number of time bins we consider.

$\bar{f}_{\text{eff}}(E)$ is the weighted average efficiency in the energy bin, and f_{cosmo} and f_{gaps} are defined in the Appendix. Using this PDF the extended (log-)likelihood is defined as

$$2 \log L(A_0, A_1, \omega, t_0) = 2 \sum_i \phi(t_i) - 2 \int_{t_{\text{start}}}^{t_{\text{end}}} dt \phi(t) , \quad (2.3)$$

where $t_{\text{start}} = -28$ days and $t_{\text{end}} = 429.9$ days for the data run in [2], and the sum is over all data points in the sample. The quantity $L(A_0, A_1, \omega, t_0)$ is maximized, subject to the constraints that $A_{0,1}$ be positive and that $0 \leq t_0 \leq \text{year}$. Again we consider various hypotheses and the significance in the data for any particular hypothesis relative to any other may be determined by studying the difference between $2 \log L_{\text{max}}$ for the two hypotheses, this difference follows a χ^2 distribution.

2.2.1 Lomb-Scargle Periodogram

The weighted Lomb-Scargle technique is ideally suited to search for periodic signals in unevenly sampled data, such as that of CoGeNT. For data that are divided into N independent time bins with $y(t_i)$ data points each ($i = 1, \dots, N$), the Lomb-Scargle power, for frequency f , is given by

$$P(f) = \frac{1}{2\sigma^2} \left(\frac{[\sum_{i=1}^N W_i (y(t_i) - \bar{y}) \cos \omega(t_i - \tau)]^2}{\sum_{i=1}^N W_i \cos^2 \omega(t_i - \tau)} + \frac{[\sum_{i=1}^N W_i (y(t_i) - \bar{y}) \sin \omega(t_i - \tau)]^2}{\sum_{i=1}^N W_i \sin^2 \omega(t_i - \tau)} \right), \quad (2.4)$$

where \bar{y} and σ are the weighted mean and variance for the data in all the time bins and ω is the angular frequency. The phase factor τ and weight factor W_i are given by

$$\tan(2\omega\tau) = \frac{\sum_{i=1}^N W_i \sin 2\omega t_i}{\sum_{i=1}^N W_i \cos 2\omega t_i} \quad \text{and} \quad W_i = \frac{1/\sigma_i^2}{\langle 1/\sigma_i^2 \rangle}, \quad (2.5)$$

respectively. Here, σ_i are the individual uncertainties in each bin.

For a given energy range, the events are divided into 80 time bins of approximately 6 days each. The contents of each bin must be sufficiently large that the error on the number of events is well approximated by a Gaussian in order for the Lomb-Scargle analysis to have a well-defined statistical interpretation. Thus, we require that each bin contains 10 or more events, and we treat the error in each bin as Gaussian, i.e. $\sigma_i = \sqrt{N_i}$. To achieve this, a simple algorithm is used to merge any bin that contains fewer than 10 events with the next highest bin³. This procedure is repeated until no bin has fewer than 10 events. In addition, the centers of the bins are shifted to take into account any dead time that may have occurred. Finally, as above, the bin contents are efficiency adjusted and the L-shell background in every bin is subtracted off, and the contents of the bin are converted to units of events/day/keVee. The error is based on the total (pre-subtraction) bin contents. This error is important for determining the weighting factors W_i . The power observed in the frequency $\omega_0 = 2\pi/1 \text{ year}$

³If the last bin has fewer than 10 events, it is merged with the penultimate bin.

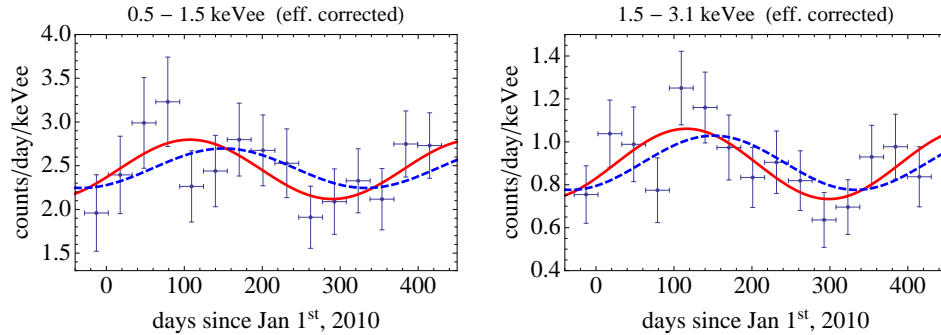


Figure 1: Time-binned data in various energy ranges. Specifically (*left*) [0.5–1.5] keVee, (*right*) [1.5–3.1] keVee. Overlaid are the best fit to the modulation, as derived using the binned analysis, with free phase (*solid red curve*) and peak set at 152 days (*dashed blue*). These best fit points correspond to $A_0 = 7.4$ (7.5) events/day/kg/keVee, $A_1 = 0.14$ (0.09) and $t_0 = 107$ (152) days, for the phase free ($t_0 = 152$ days) for the lower bin and $A_0 = 2.7$ (2.7) events/day/kg/keVee, $A_1 = 0.18$ (0.14) and $t_0 = 116$ (152) days for the higher.

can be converted to a significance for an oscillating signal. The probability of observing power P at any particular frequency in data that do not contain any oscillating signal is e^{-P} , whereas the probability for observing power P at *any* frequency (including the appropriate trial factor) is approximately given by $1 - (1 - e^{-P})^N$, where N is the number of time bins [29].

3. A Study of Modulation

The central question we wish to understand is the properties of any annual modulation present in the data. As such, we begin by applying the statistical techniques presented above to analyze the properties of the modulation in the CoGeNT data, without any assumptions of its origin. To begin, we have reproduced the results in [2], where a time-binned analysis was done in the energy ranges 0.5–0.9 keVee and 0.5–3.0 keVee. These plots, and the results of [2], suggest that the region above 0.9 keVee exhibits a sizeable component of the modulation, so we divide the energy into two exclusive regions: a “low region” [0.5–1.5 keVee] and a “high region” [1.5–3.1 keVee], shown in Figure 1.

The data clearly exhibit a modulation over a wide range of energies. The significance of adding a modulating term with a free phase (2 parameters), relative to the null hypothesis of no modulation, is $\Delta\chi^2 = 4.7$ in the range [0.5–1.5] keVee, and 8.2 in the range [1.5–3.1] keVee. Furthermore, the improvement in $\Delta\chi^2$ arising from adding a cosine with fixed phase (1 parameter) is 2.3 for the [0.5–1.5] keVee range, and 5.2 for [1.5–3.1] keVee. There is strong support for modulation in the high energy range, with little benefit in the low range. In addition, the high energy region prefers a phase that is different from that expected for a Maxwellian halo.

The modulation in energies above 1.5 keVee is surprising, as the rate spectrum in this region had previously been interpreted as a constant background contribution [1]. The unex-

pected nature of this modulation warrants a careful analysis of its properties and in the next two subsections, we apply additional tests to study its period, phase and amplitude. The last subsection presents the energy spectrum for the unmodulated and modulated rates as well as for the phase, assuming an oscillation period of a year.

3.1 Oscillation Period

Before moving on to the questions related to annual modulation, it is important to check whether other key time periods show up in the data. The most obvious to check is evidence for daily modulation. While the daily modulation expected from dark matter is negligible in a detector like CoGeNT, many sources of background, such as those induced by cosmic rays, can depend on the time of day.

We study this in figure 2, which shows the significance of modulation, both under the assumption that the oscillation period is one solar day (24 hrs) and under the assumption that it is one sidereal day (23.93 hrs). The plots show results for different energy ranges $[E_{\text{low}}-E_{\text{high}}]$, where E_{low} and E_{high} have been varied between 0.5 and 3.0 keVee in steps of 0.1 keVee. Even though our best-fit solutions typically include about 10–20% modulation, the statistical significance is very small, as indicated by the p -values in the plots. While there are a few isolated energy intervals in which modulation appears to be established at more than 2σ confidence, we remark that, once the trial factor for this to happen anywhere in the considered energy range is included, the significance becomes much lower. We thus conclude that the CoGeNT data do not show evidence for diurnal modulation.

More generally, we can also search for modulation with any frequency using the Lomb-Scargle technique. The results are shown in figure 3. From the left panel, we read off that the strongest modulation in the data indeed has a period of 1 year. The Lomb-Scargle significance for annual modulation is above 3σ if no trial factor is included, and around 90% if we allow for a trial factor. In the right panel of figure 3, we show the significance of annual modulation, defined as the probability of obtaining the observed annual modulation from statistical fluctuations alone (not including a trial factor), as a function of the considered energy range $[E_{\text{low}}-E_{\text{high}}]$. We find that there is no significant modulation below ~ 1.7 keVee, but that the significance increases once higher energies are included.

3.2 Phase and Amplitude for Annual Modulation

Before moving on to model-dependent analyses, it is worth understanding the significance, phase, and size of the signal present in the data, irrespective of any appeal to particle physics or astrophysics model. We thus proceed to consider the phase and amplitude of the modulation for a constant period of one year. An unbinned (in time) log-likelihood analysis was done for three energy ranges: low [0.5–1.5] keVee, high [1.5–3.1] keVee, and all [0.5–3.1] keVee. Figure 4 shows that the high energy data carry nearly the full weight of the analysis, and that the preferred phase is not Maxwellian, confirming the results of the binned analysis in Fig. 1. The modulation fraction in the high energy range is $\sim 20\%$, with a phase around 106 days.

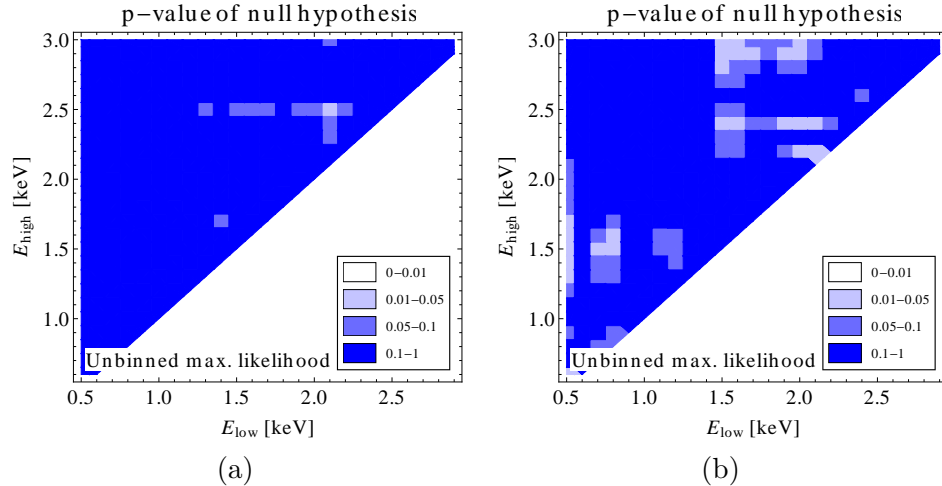


Figure 2: Significance of daily modulation in CoGeNT, as measured by the probability for the null (no modulation) hypothesis to give the observed amount of modulation. We have fitted a model of the form (2.1) to the data after subtracting backgrounds and correcting for detection efficiencies and shutdown periods. In the fit, we have kept the oscillation period ω fixed at (a) one solar day (24 hrs) and (b) one sidereal day (23.93 hrs), and we have treated the average rate A_0 , the modulation fraction A_1 , and the phase t_0 as free parameters.

Figure 5 shows the significance of modulation over the null hypothesis in a range of energies from some initial energy, E_{low} , to some final energy, E_{high} , where $E_{\text{low}}, E_{\text{high}}$ each go from 0.5 to 3 keVee in steps of 0.1 keVee. The results for both the binned (left-hand column) and unbinned (right-hand column) analyses are shown to illustrate that the two methods are in very good agreement. We consider the significance when the phase is allowed to float, upper plots, and when the phase is fixed to that expected from the SHM ($t_0 = 152$ days), lower plots.

The smallest p-values for the null hypothesis occur in the energy range 0.5–3.0 keVee. As in figure 3 (b), we find that there is no significant modulation from $E_{\text{low}} = 0.5$ to $E_{\text{high}} \sim 1.7$ keVee, but the significance starts to increase as $E_{\text{high}} \gtrsim 1.7$ keVee. In the energy range where the modulation appears to be most significant, the phase and modulation fraction are both relatively stable; the best-fit phase falls consistently from 60–120 days, while the best-fit modulation fraction falls between 10-20%, for fits over the full energy range (0.5–3.0 keVee).

3.3 Spectra

Having properly understood the presence and basic properties of the modulation, we move on to understand better in what energy range it lies. Thus, we proceed here to derive the energy spectra of the unmodulated and modulated rate components, and the oscillation phase. The data are divided into four energy bins: [0.5–0.9], [0.9–1.5], [1.5–2.3] and [2.3–3.1] keVee. This separates the data into a bin dominantly below the cosmogenic peaks, one encompassing the cosmogenic background, and two evenly spaced bins above the cosmogenic peaks. For each

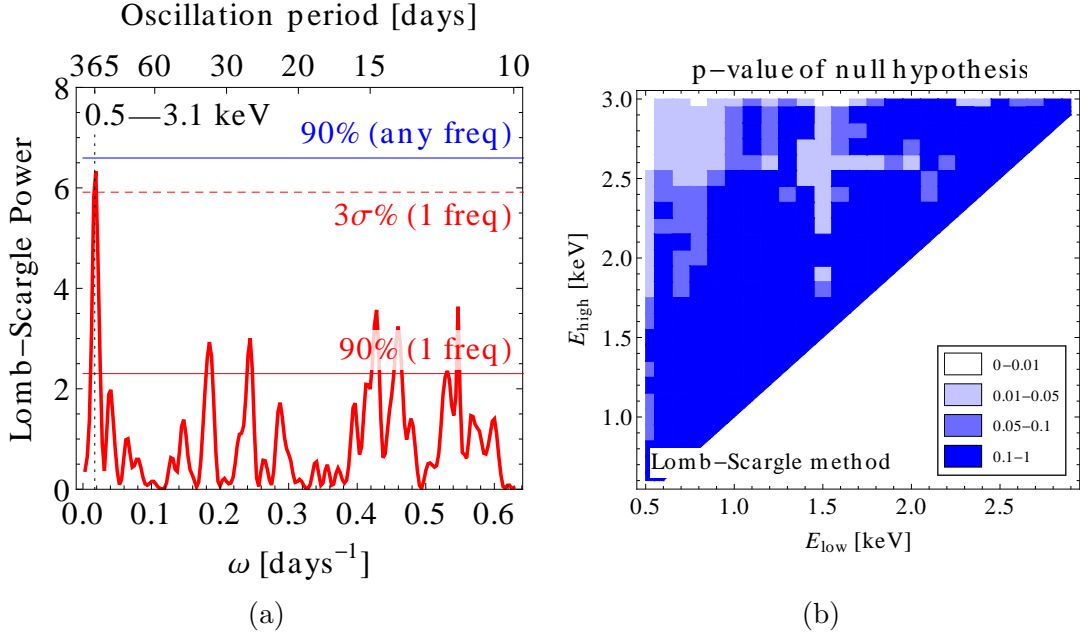


Figure 3: Results of the Lomb-Scargle analysis. In the left panel, we show the Lomb-Scargle periodogram for the full energy range 0.5–3.1 keV, whereas in the right panel we plot the significance of annual modulation as a function of the considered energy range.

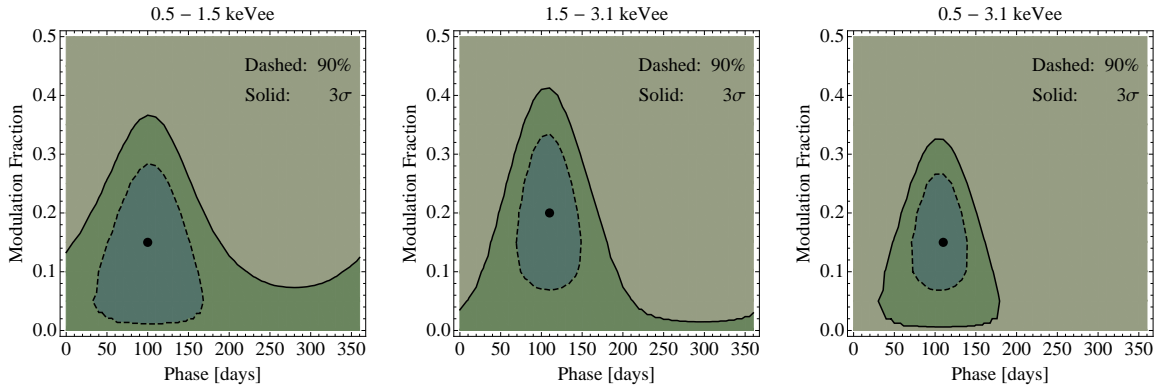


Figure 4: Likelihood analysis of the allowed regions in modulation and phase for different energy ranges: in [0.5–1.5] keV (*left*), [1.5–3.1] keV (*middle*), and [0.5–3.1] keV (*right*). The contours are of $\Delta\chi^2$ from the best fit point, shown as \bullet .

bin, an unbinned (in time) log-likelihood approach is used to obtain the best-fit values for the unmodulated rate (A_0), modulated amplitude ($A_0 * A_1$), and phase (t_0).

Figure 6 shows the best-fit values as a function of energy, once the period is fixed to one year. Three different scenarios are considered: (blue) the phase is set to Maxwellian ($t_0 = 152$ days), (green) the phase is fixed to the best-fit value for the fit over 0.5–3.1 keV ($t_0 = 106$ days), and (red) the phase is allowed to float bin-by-bin. Note that both the

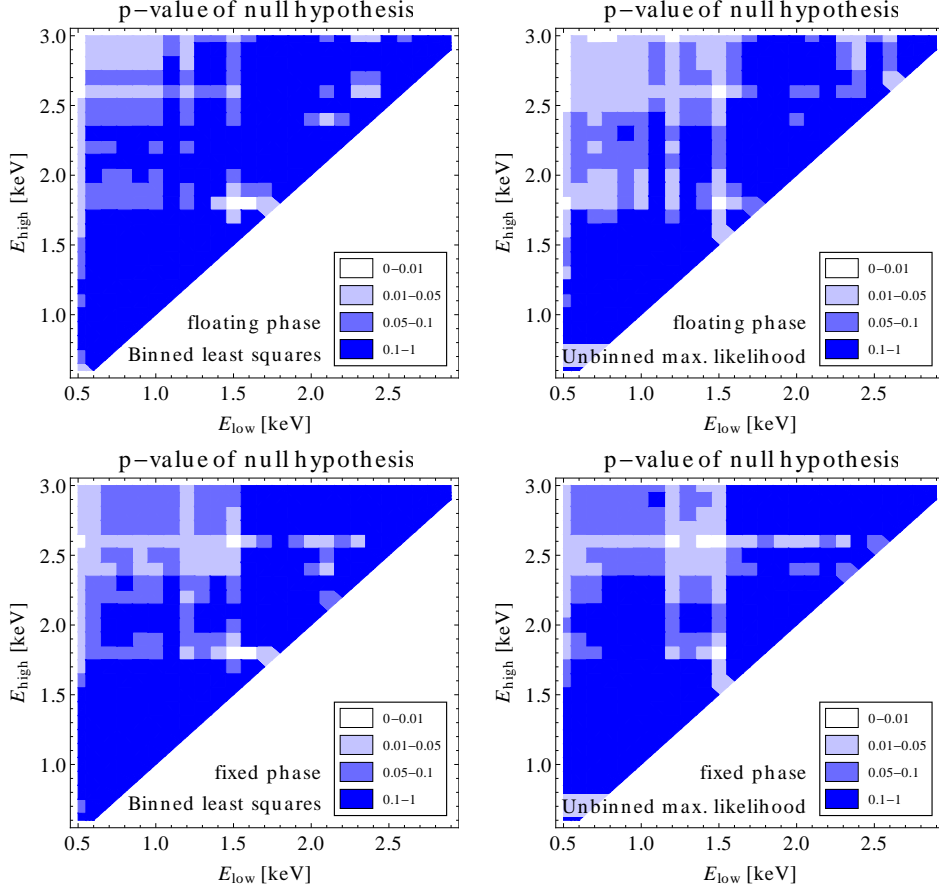


Figure 5: Results of modulation fit with $\omega = \omega_0 = 2\pi/1$ year, using both the binned and unbinned approaches. The upper plots allow the phase to float and the lower plots fix it at the value expected by the SHM ($t_0 = 152$ days). The probability of the null (no modulation) hypothesis to fluctuate to the observed best fit values is calculated from the $\Delta\chi^2$ between the two best fits, assuming 2 degrees of freedom for the upper plots and 1 for the lower.

unmodulated rates and the modulation amplitudes do not differ too dramatically between these three scenarios. The modulated amplitude has a large value (~ 1.5 cpd/kg/keVee) in the lowest energy bin, but very large error bars (± 0.8 cpd/kg/keVee). The modulation amplitude flattens out considerably at higher energies around ~ 0.5 cpd/kg/keVee, with smaller error bars. When the phase is allowed to float, it remains relatively stable over the full energy range, with small variations around the best-fit value. The significance is highest in the last energy bin for the floating and best-fit phase scenarios; it is largest in the second to last energy bin for the Maxwellian case.

The fact that the modulation amplitude in Fig. 6 is non-zero even at large energies is a non-trivial and important feature of the spectrum. To see if this modulation amplitude eventually “turns off,” we have also analyzed CoGeNT’s high energy channel. The low and high energy channels in the data both measure pulse amplitudes in the range from 0.05 V

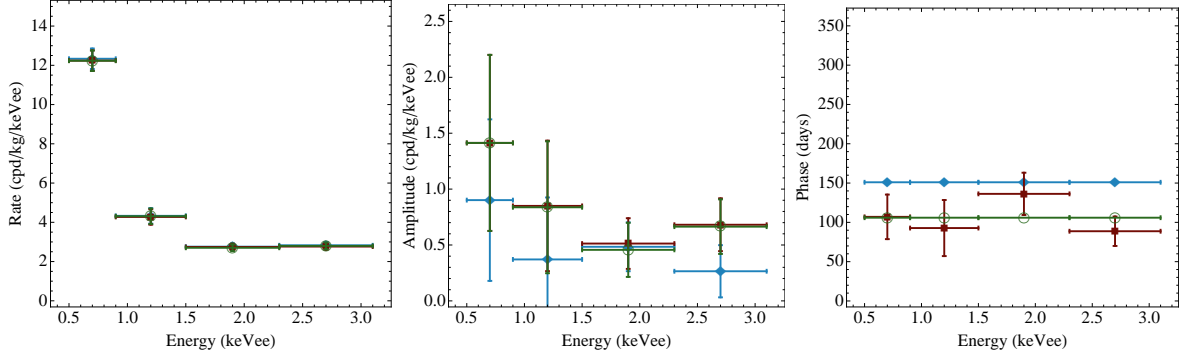


Figure 6: Spectra for three different scenarios: (red square) the phase is allowed to float in the fit, (blue diamond) the phase is fixed to Maxwellian (152 days), and (green open circle) the phase is fixed to the best fit phase (106 days) for a fit to the full data range 0.5-3.1 keVee. The spectra represent: total rate (left), modulation amplitude (middle) and phase (right).

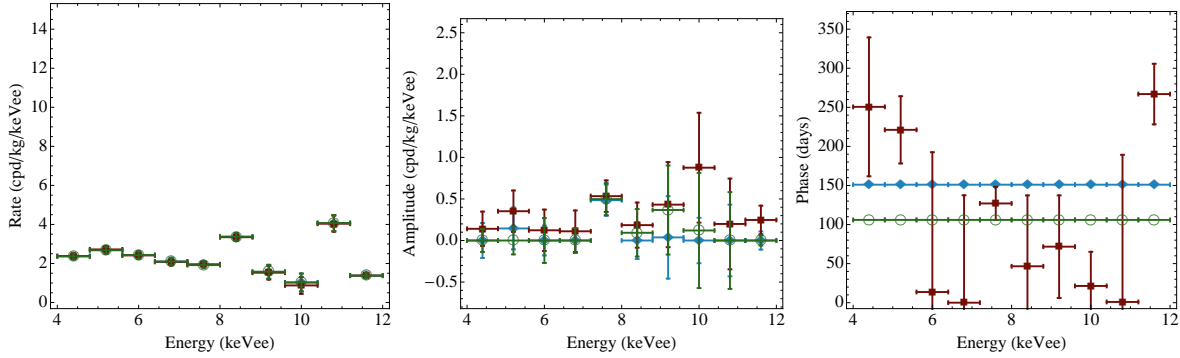


Figure 7: Same as Fig. 6, except for data from the high energy channel.

and 0.25 V. However, the relation between the actual physical energy deposited and the measured voltage is different for the two channels. In particular, the response function at high energies is optimized to provide a good fit to the K-shell cosmogenics from ~ 4 -12 keVee (see Appendix A for a more complete discussion of the modeling of these cosmogenics), but is not optimized for energies below ~ 3.2 keVee. Figure 7 shows the results of a log-likelihood analysis in equally-spaced bins above 4 keVee. The unmodulated rate spectrum indicates that there is an unexplained excess of events that is fairly constant with energy. In contrast to the low energy channel, the phase is highly unconstrained above ~ 4 keVee when it is allowed to float in the fitting procedure. This is due to the fact that there is no significant modulation in this energy regime, as illustrated by the spectrum of the modulation amplitude.

Figure 6 shows that there is some modulation in the energy bin from 0.9-1.5 keVee, where the L-shell cosmogenic peaks are expected to dominate. As a check that the most dominant of these peaks, Ge^{68} , is not oscillating, we plot the time-binned data for energies centered on this peak in Fig. 8 (red open circles). The black diamonds in the figure show the expected exponentially falling background, modeled using the procedure described in Appendix A. The

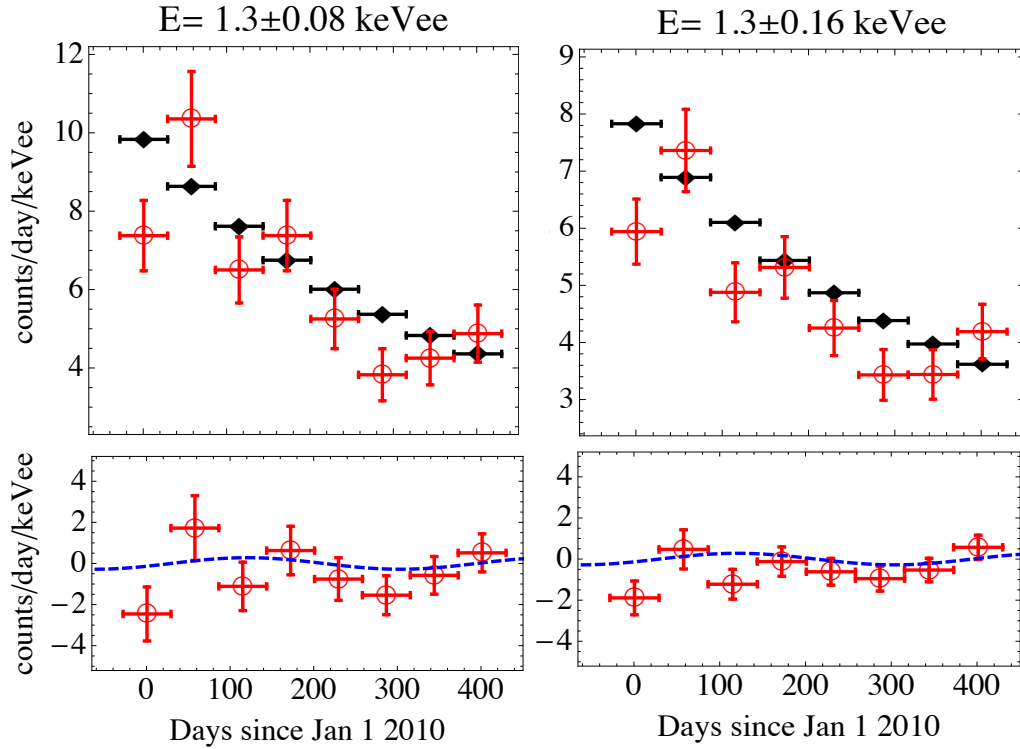


Figure 8: Time variation for data centered on the Ge^{68} L-shell peak for two different energy ranges. The top panel shows the predicted cosmogenic contribution using Eq. A.1 and the parameters given in Appendix A (black diamonds), as well as the (efficiency corrected) time-binned distribution of the data (red open circles). A constant of 1.4 counts/day/keVee (see unmodulated spectrum in Fig. 6) has been added to the background. The bottom panel shows the residuals between the data and the model (red). The dashed blue line is the best-fit modulation in the range 0.9–1.5 keVee, obtained using the log-likelihood approach as in Fig. 6.

bottom panel in the figure shows the residual between the data and model, overlaid with the best-fit modulation in the 0.9–1.5 keVee energy bin from Fig. 6. As the energy range about $E = 1.3$ keVee is widened, the residuals come into better agreement with the blue line. In the narrow energy band, the statistics are too large to conclude whether there is a larger modulating component on the peak. As more data are collected and the statistics improve, it will be crucial to study the time variation of the Ge^{68} line to understand whether additional cosmogenics have contaminated the detector since the start of the experiment.

4. A Dark Matter Interpretation

4.1 Dark Matter Fit for Standard Halo Parameters

The statistical analysis of the modulation in the previous section suggests that its distribution, as a function of energy, is not indicative of a conventional elastically-scattering WIMP.

Furthermore, the phase of the modulation does not appear completely consistent with that expected from the standard halo model (SHM). However, there are uncertainties associated with these statements and so we will explore various different particle physics models in this section to see what best fits the observed data. Unless specified, we will assume that the velocity distribution of the dark matter is Maxwell-Boltzmann with velocity dispersion $v_0 = 220$ km/s and escape velocity $v_{\text{esc}} = 550$ km/s:

$$f(v) \propto (e^{-v^2/v_0^2} - e^{-v_{\text{esc}}^2/v_0^2}) \Theta(v_{\text{esc}} - v) , \quad (4.1)$$

where v is the velocity in the galactic rest frame. We will consider more general velocity profiles in the following subsections.

We have carried out fits using an unbinned extended maximum likelihood approach and a binned χ^2 analysis. For the unbinned method, we define a likelihood function that includes the dark matter signal, the cosmogenic backgrounds, and a constant background with floating normalization. The likelihood function accounts for efficiencies and shutdown periods. For the binned approach, we have divided the data into 5 energy bins of equal size, spanning the range from 0.5–3.0 keVee. Within each energy bin, the events are partitioned in 15 equal-sized time bins, each approximately one month wide. We have subtracted cosmogenic backgrounds and have corrected for the shutdown periods of the detector (the efficiencies are accounted for in the predicted dark matter signal). The error in each bin is based on the statistical uncertainty before background subtraction and live time correction, and is assumed to be approximately Gaussian, which is a reasonable assumption because no bin has fewer than six events. We carry out a χ^2 fit to these 75 bins, minimizing over dark matter parameters and systematic nuisance parameters.

We have considered several different signal and background scenarios and found the associated significance for each in the data. The results are summarized in Table 1 and should be compared to a background-only fit where a constant rate is assumed in each of the five energy bins with no time variation. This fit gives $\chi^2 = 58.2$ for the 70 degrees of freedom.

- **Spectrum + Modulation** We attempt fitting elastic DM (eDM), varying σ and m_χ , to both the energy spectrum and its time dependence. We assume an additional background contribution, constant in time and energy, and include its rate as a nuisance parameter, c_0 . The binned analysis gives $\chi^2 = 57.3$ for 72 d.o.f.. The predicted and observed rates for the best-fit point obtained from the unbinned method is also shown in figures 9 and 10. The best-fit for the eDM scenario, which has a mass ~ 7 GeV, is marginally better than the time-independent background-only fit; the corresponding p-value is 0.64.
- **Spectrum Only** The second column of Table 1 shows an eDM scenario with a constant background, but this time fitting only to the unmodulated spectrum, i.e. ignoring time information. In this case, the binned least-squares analysis uses 50 bins and gives $\chi^2 = 50.8$ for 47 d.o.f..

Scenario	Spect+Mod		Spect only		Mod only ($c_i \geq 0$)		iDM Mod only
d.o.f.	72	[n/a]	47	[n/a]	68	68	67
$\sigma/10^{-41}$ cm ²	13.8	[8.9]	10.1	[8.2]	6.0	8.6	64
m_χ / GeV	7.2	[8.1]	7.7	[8.2]	10.0	12.0	16.3
δ / keV							24
c_i /(cpd/kg/keVee)	2.5	[2.5]	2.5	[2.6]	$\begin{pmatrix} 1.5 \\ 0 \\ 1.5 \\ 2.3 \\ 2.3 \end{pmatrix}$	$\begin{pmatrix} -5.9 \\ -4.6 \\ -1.0 \\ 1.1 \\ 1.7 \end{pmatrix}$	$\begin{pmatrix} 8.7 \\ 0.4 \\ 0.4 \\ 1.2 \\ 1.5 \end{pmatrix}$
χ^2	57.3	[n/a]	50.8	[n/a]	53.7	51.4	51.3

Table 1: The best fit DM parameters for the binned [unbinned] analyses of various DM scenarios. The numbers should be compared to a background-only fit that gives $\chi^2 = 58.2$ for the 70 degrees of freedom (see text for details).

- **Modulation Only** The third and fourth columns of Table 1 only fit to the modulation in the data. The fits are done for an eDM plus background hypothesis, where the time-independent background is allowed to vary freely in each of the five energy bins (i.e., there are five nuisance parameters c_i). For the case where these constant contributions, presumably coming from some unidentified background, are restricted to be physical, i.e. $c_i \geq 0$, we find a fit that gives $\chi^2 = 53.7$ for 68 d.o.f. If instead they are allowed to float entirely, we find $\chi^2 = 51.4$, again with 68 d.o.f. Notice that when fitting the modulation, the best-fit dark matter mass is $\sim 10 - 12$ GeV.

It is clear from Table 1 that although the data are consistent with the SHM DM hypothesis, the inclusion of such a DM component does not greatly improve the fit compared to the hypothesis of a background that is constant in time. Furthermore, there is slight tension in the DM interpretation—the modulation in the data by itself favors heavier dark matter masses than the spectrum. This behavior is also illustrated in Figure 11, where we show the preferred region in DM mass m_χ and elastic spin-independent scattering cross section σ_{SI} for various fits to the CoGeNT data. The plot confirms the slight (but not statistically significant) tension between the DM masses preferred by the energy spectrum observed in CoGeNT and the annual modulation. A fit to the modulation data alone can exclude the hypothesis of no DM at low confidence level (light red contours), however this requires an unphysical background (i.e., unphysical negative background, $c_i \leq 0$).⁴ If positive background is required, the modulation provides only an upper bound. We also compare the CoGeNT-preferred regions to the exclusion limits from Xenon-100 [9] and CDMS [15], and confirm the well-known

⁴This somewhat unphysical approach has been chosen in ref. [30], which is one of the reasons why some of their conclusions differ from ours.

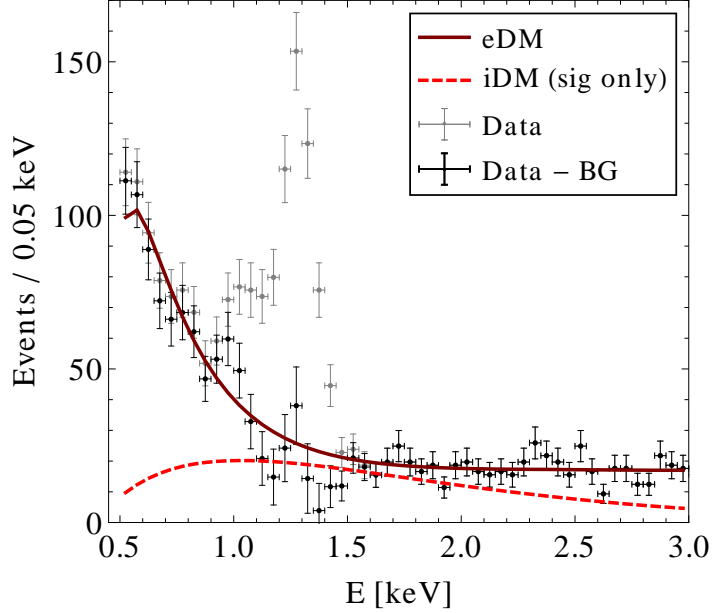


Figure 9: Comparison of the CoGeNT data to the predicted event spectrum for elastically (solid dark red) and inelastically (light red dashed) scattering dark matter. In both cases, results for the best fit dark matter parameter are shown. In the elastic case, the fit was done using the unbinned maximum likelihood approach including energy and timing information for each event as well as a constant background, whereas in the inelastic case, we have carried out the binned analysis described in the text, with 5 constant backgrounds c_i . (For iDM, only the signal is shown, but not the fitted constant background.)

tension between these results. We also compare to the DM parameter region favored by the DAMA experiment [7]. In computing this region, we mostly follow the procedure described in [31], assuming no channeling [32, 33] and assigning a 10% systematic uncertainty to the DAMA quenching factors [34, 35, 30]. This systematic uncertainty has a strong impact on the horizontal extent of the DAMA region. We find that for standard halo parameters, the DM interpretations of DAMA and CoGeNT are inconsistent. To some extent, this tension can be relaxed for halo parameters different from the ones we chose in figure 11 [36, 37]. In addition, one might speculate that systematic uncertainties in either DAMA or CoGeNT could be larger than what we assumed. For instance, if the low-energy event excess in CoGeNT was only partly due to dark matter and partly due to some other source, the CoGeNT-allowed regions could shift to higher mass.

Because an elastically scattering WIMP with a Maxwell-Boltzmann velocity distribution only produces a large modulation amplitude at low energies ($\lesssim 1.5$ keVee), which is not what is observed at CoGeNT, it is worthwhile considering non-standard WIMP scenarios as an explanation of the CoGeNT modulation. Inelastic dark matter (iDM) is an example of a DM scenario with increased modulation and a preference for events at high recoil energy [38]. We

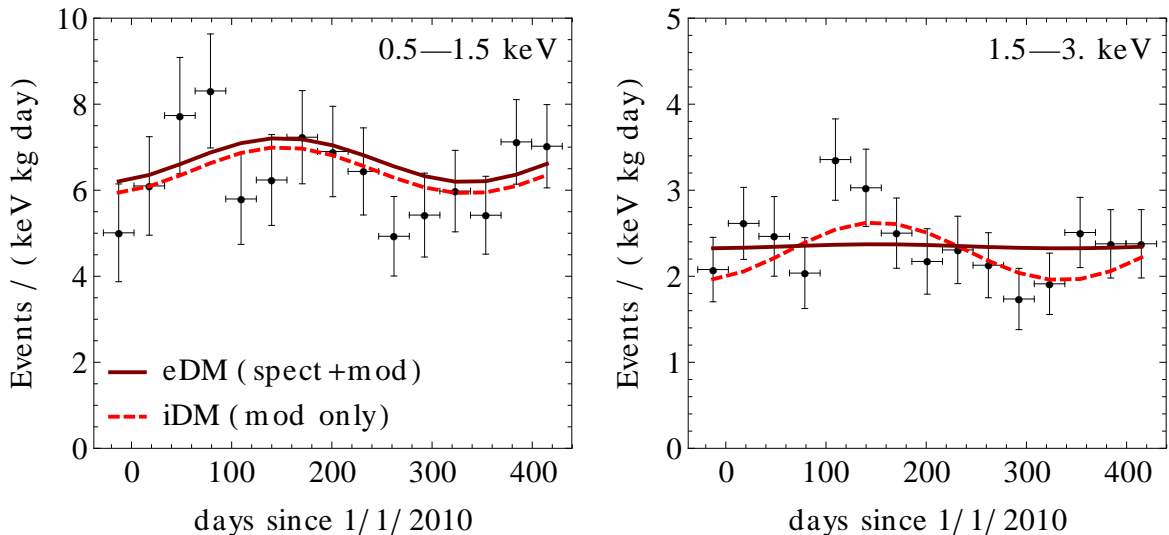


Figure 10: Comparison of the CoGeNT data to the predicted time-dependent event rate for elastically (solid dark red) and inelastically (light red dashed) scattering dark matter, using the same fitting procedures as for fig. 9.

can repeat the exercise above under the assumption that DM scatters inelastically. However, there is no preference for iDM from fits to the unmodulated spectrum, which has many events below where an inelastic contribution is expected - see figure 9. There is, however, a preference for iDM if one fits to only the modulation (see last column in Table 1). Interestingly, once iDM is taken as the DM hypothesis, there is no improvement in the fit if the background is allowed to be unphysical ($c_i < 0$). Instead, the iDM model enables a similar modulation spectrum as the eDM fit, but with physical backgrounds. For the modulation only fit we find that iDM gives $\chi^2 = 51.3$ for 67 d.o.f. The spectra at this best-fit point are shown in Figure 10, and we can conclude from this figure that iDM can produce modulation in all energy bins, but at the cost of explaining only part of the event excess observed by CoGeNT. We note that inelastic WIMPs are highly sensitive to non-Maxwellian properties. If the phase is truly shifted away from 152 day peak, this could be indicative of such halo properties. Remarkably, the best-fit phase is mid-April, in a time when XENON100 had increased levels of noise and consequently a signal localized in time to that period could have been missed. Since iDM in the presence of a stream can lead to narrow peaks, and only for brief periods of the year [39], further running of XENON100 overlapping April should clarify this.

4.2 Varying the Halo Parameters

Next, we explore whether the CoGeNT data are compatible with a general class of equilibrium velocity distributions that extend beyond Maxwell-Boltzmann. In particular, we consider

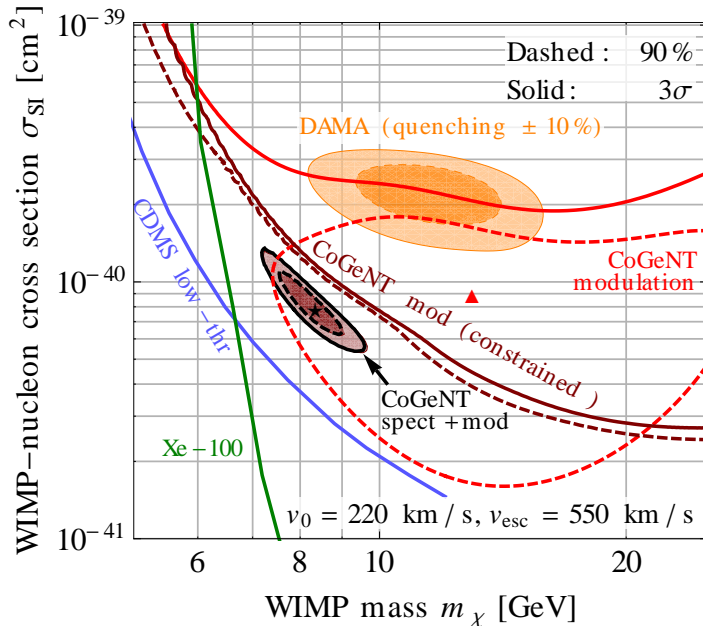


Figure 11: Preferred regions and exclusion limits at 90% and 3σ confidence level in the m_χ - σ plane for spin-independent dark matter–nucleon scattering assuming a standard Maxwell-Boltzmann halo with escape velocity $v_{\text{esc}} = 550$ km/s and velocity dispersion $v_0 = 220$ km/s. Filled red (dark gray in B/W) contours were obtained from an unbinned maximum likelihood fit to the CoGeNT data, using both the energy and timing information for each event. (A fit using only energy information gives practically identical results.) The unfilled red (gray) contours are from a binned χ^2 analysis, using only the timing information and leaving the energy spectrum completely unconstrained (light red/light gray contours), or requiring the predicted energy spectrum to remain below the observed one (dark red/dark gray exclusion limits). The orange (light gray) region shows the masses and cross sections preferred by DAMA [7] if the quenching factors are assigned a 10% uncertainty [31, 35, 30], and the blue and green contours indicate the 90% exclusion limits from CDMS [15] and Xenon-100 [9], respectively.

distributions of the form

$$f(v) \propto (e^{-v^2/v_0^2} - e^{-v_{\text{esc}}^2/v_0^2})^k \Theta(v_{\text{esc}} - v), \quad (4.2)$$

where k is a power-law index, v_{esc} is the escape velocity, and v_0 is the dispersion. Note that $k = 1$ is just the Maxwell-Boltzmann-like halo. This velocity distribution models the behavior of double power-law density profiles and corresponds to results found in high-resolution simulations of the Galactic halo, when $k \sim 2$ [37]. The fact that simulations support a power-law index greater than one suggests that the number of high velocity particles on the tail of the distribution may be suppressed relative to the expectation for Maxwell-Boltzmann halos.

To study how the CoGeNT predictions are affected by variations in the halo parameters, distributions with $k = 1, 2, 3$ are considered and a random scan is done with $v_{\text{esc}} \in [500, 600]$

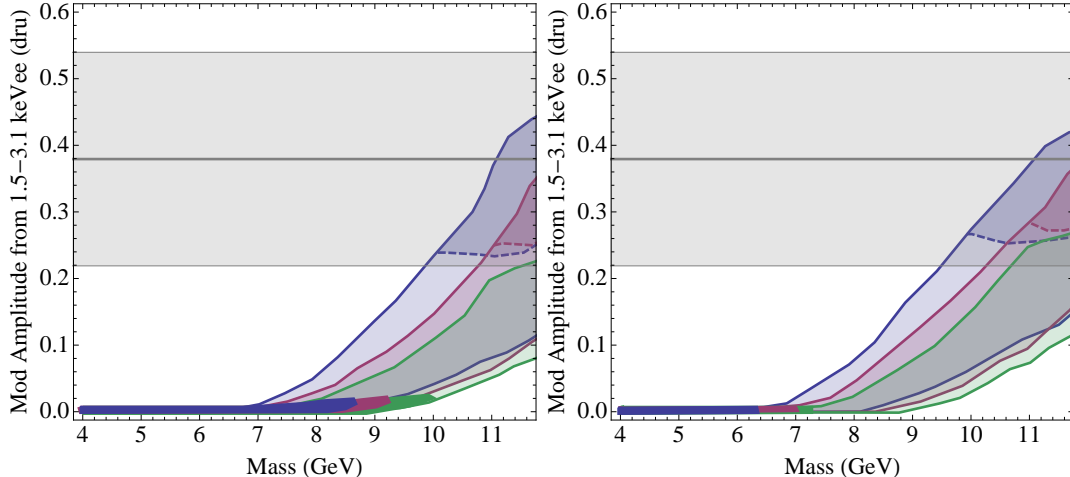


Figure 12: Modulation amplitude in the range 1.5–3.1 keVee as a function of dark matter mass, where the dark matter cross section is normalized to the modulation amplitude in the first bin (left) and over the whole energy range (right). The colors indicate different spectral indices for Eq. 4.2: $k=1$ (blue), $k=2$ (pink), $k=3$ (green). The regions between (above) the solid (dashed) lines indicate points that overpredict the unmodulated rate within 2σ from 0.5–1.5 keVee (1.5–3.1 keVee). The solid colored bands are the only regions consistent with the unmodulated rate spectrum. The gray band is the modulated amplitude with 1σ error bars for the 1.5–3.1 keVee region.

km/s [40] and $v_0 \in [180, 280]$ km/s [41, 42, 43]. For each randomly selected set of halo parameters and dark matter mass, the modulated and unmodulated rates are evaluated in two energy bins: 0.5-1.5 keVee and 1.5 - 3.1 keVee. The results are summarized in Fig. 12 for the case where the cross section is normalized to give the measured modulation amplitude in the first bin (left) and the case where it is normalized to the total amplitude from 0.5-3.1 keVee (right). The three colors represent three different spectral indices, with $k=1$ Maxwellian-type in blue, $k=2$ in pink, and $k=3$ in green. The gray band is the best-fit modulation amplitude ($\pm 1\sigma$ error bars) for 1.5-3.1 keVee, obtained using the log-likelihood method.

The data support a modulation amplitude of $\sim 0.38 \pm 0.16$ cpd/kg/keVee in the high energy bin. For the elastic scattering case considered here, only dark matter masses greater than ~ 9 GeV for $k=1$ and ~ 10.5 GeV for $k=3$ yield a modulation amplitude within a standard deviation of the measured value. While a heavier dark matter mass increases the modulation amplitude at high energies, it also increases the unmodulated rate, making it conflict with the rates measured by CoGeNT. For the wide range of halo and dark matter parameters considered here, only masses less than $\sim 7 - 9$ GeV are consistent with CoGeNT’s unmodulated spectrum. Unfortunately, none of these points give a sufficient modulation at high energies. The results shown here emphasize the underlying tension in a dark matter interpretation of the CoGeNT data: namely, one must explain both an excess in the unmodulated rate below ~ 0.9 keVee and a significant modulation above ~ 1.7 keVee. As Fig. 12 highlights, a dark matter candidate scattering elastically off an equilibrated halo cannot satisfy both

requirements.

4.3 Model Independent Comparisons

With the presence of modulation in the high energy data, but the exponential signal in the low energy data, it seems difficult to find a spin-independent elastic DM model that can explain all features simultaneously. However, this does not mean that it is impossible. In particular, some especially exotic halo model might exist that might allow consistency. The fact that the best fit phase seems quite different from what is expected in a Maxwellian velocity distribution would seem additionally to point to some exotic halo component, such as a stream.

Since both detectors contain germanium, a simple and direct comparison can be made between CoGeNT and CDMS-Ge by comparing the count rates at CoGeNT to those from the low-energy analysis of the CDMS experiment [15]. We make this comparison by calculating an upper limit in each detector, such that the probability of having a lower rate is 1.3%. Then the probability that any one out of the 8 CDMS detectors should have observed a rate lower than its observed rate is 10%. Then, in each bin, we take the strongest limit from among all of the detectors and treat that as a 90% confidence limit. (Note that the probability that the particular detector that sets the limit happened to have a strong downward fluctuation is small, and so the confidence is actually better than 90%, but we treat it as a 90% C.L. to be conservative.)

We show these limits in figure 13. We see that the count rates at CDMS are not low enough to constrain the CoGeNT modulation. However, the count rates *are* low enough that there should be modulation at a very high level in CDMS. Thus, even weak modulation constraints from CDMS could be very powerful, or conversely, even at their existing count rates, modulation should be apparent in a dedicated modulation analysis.

Comparing to other targets may seem more challenging. However, a means of directly comparing different experiments independent of halo models has recently been proposed [44]⁵. The idea is quite simple, in particular for elastic spin-independent scattering. In this case, the signal appearing in the range $[E_{low}^{(1)}, E_{high}^{(1)}]$ at experiment 1 can be expected to arise in experiment 2 in the energy range

$$[E_{low}^{(2)}, E_{high}^{(2)}] = \frac{\mu_2^2 M_T^{(1)}}{\mu_1^2 M_T^{(2)}} [E_{low}^{(1)}, E_{high}^{(1)}], \quad (4.3)$$

where $M_T^{(i)}$ are the masses of the target nuclei in each experiment and μ_i is the DM-nucleus reduced mass for each experiment. For a rate, dR_1/dE_R , observed at experiment 1, the rate expected at experiment 2 is

$$\frac{dR_2}{dE_R}(E_2) = \frac{C_T^{(2)}}{C_T^{(1)}} \frac{F_2^2(E_2)}{F_1^2\left(\frac{\mu_1^2 M_T^{(2)}}{\mu_2^2 M_T^{(1)}} E_2\right)} \frac{dR_1}{dE_R}\left(\frac{\mu_1^2 M_T^{(2)}}{\mu_2^2 M_T^{(1)}} E_2\right). \quad (4.4)$$

⁵For related work see [45].

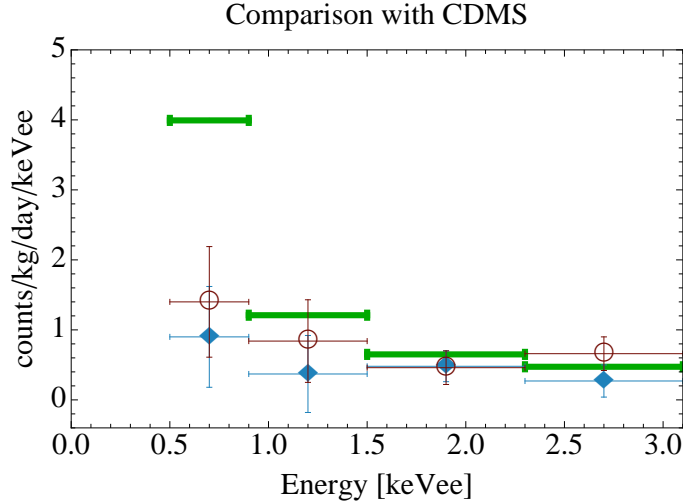


Figure 13: Upper limits from CDMS (*green*) compared with modulation rates from CoGeNT assuming a Maxwellian phase (*blue*) and the overall best fit phase (*red*).

Bin	CoGeNT	Ge	Na (Q=0.3)	Si	O	Xe
1	[0.5,0.9] 0.90 ± 0.72	[2.3,3.8] 0.23 ± 0.18	[1.5,2.5] 0.078 ± 0.062	[4.5,7.6] 0.035 ± 0.028	[5.8,9.9] 0.011 ± 0.009	[1.4,2.3] 0.72 ± 0.58
2	[0.9,1.5] 0.37 ± 0.55	[3.8,6.1] 0.1 ± 0.149	[2.5,4.0] 0.035 ± 0.052	[7.6,11.9] 0.015 ± 0.023	[9.9,15.6] 0.005 ± 0.008	[2.3,3.7] 0.31 ± 0.46
3	[1.5,2.3] 0.48 ± 0.22	[6.1,8.9] 0.136 ± 0.063	[4.0,5.8] 0.049 ± 0.022	[11.9,17.5] 0.021 ± 0.01	[15.6,22.8] 0.007 ± 0.003	[3.7,5.4] 0.41 ± 0.19
4	[2.3,3.1] 0.27 ± 0.23	[8.9,11.6] 0.08 ± 0.068	[5.8,7.6] 0.029 ± 0.025	[17.5,22.8] 0.013 ± 0.011	[22.8,29.8] 0.004 ± 0.004	[5.4,7] 0.23 ± 0.2

Table 2: Modulation amplitudes, for all columns except that labelled CoGeNT the units are counts/day/kg/keVnr, in the CoGeNT column the units are counts/day/kg/keVee, for four bins assuming a Maxwellian phase, the equivalent energy ranges and rates for other targets, assuming $m_\chi = 7$ GeV and spin-independent scattering cross sections proportional to A^2 . Note that we have not included detector efficiencies or mass fractions in any of the predicted rates.

Here

$$C_T^{(i)} = \kappa^{(i)} \left(f_p Z^{(i)} + f_n (A^{(i)} - Z^{(i)}) \right)^2, \quad (4.5)$$

and κ is the mass fraction for the target element in question, and F_i are the nuclear form factors at each experiment.

The energy ranges [0.5,1.5] and [1.5, 3.1] keVee at CoGeNT should be properly thought of as [2.3,6.1] and [6.1,11.6] keVnr in terms of nuclear recoil energies. For a WIMP of a given mass, the signals in these bins should show up in a very specific range of energies at other experiments. In tables 2 and 3 we show what energy ranges and rates should show up at other experiments for a 7 GeV WIMP, assuming a spin-independent scattering proportional

Bin	CoGeNT	Ge	Na (Q=0.3)	Si	O	Xe
1	[0.5,0.9] 1.4 ± 0.79	[2.3,3.8] 0.36 ± 0.2	[1.5,2.5] 0.12 ± 0.07	[4.5,7.6] 0.054 ± 0.03	[5.8,9.9] 0.018 ± 0.01	[1.4,2.3] 1.1 ± 0.6
2	[0.9,1.5] 0.84 ± 0.59	[3.8,6.1] 0.23 ± 0.16	[2.5,4.0] 0.079 ± 0.055	[7.6,11.9] 0.035 ± 0.024	[9.9,15.6] 0.012 ± 0.008	[2.3,3.7] 0.70 ± 0.49
3	[1.5,2.3] 0.46 ± 0.24	[6.1,8.9] 0.13 ± 0.068	[4.0,5.8] 0.047 ± 0.024	[11.9,17.5] 0.021 ± 0.011	[15.6,22.8] 0.007 ± 0.004	[3.7,5.4] 0.39 ± 0.21
4	[2.3,3.1] 0.66 ± 0.24	[8.9,11.6] 0.20 ± 0.07	[5.8,7.6] 0.072 ± 0.026	[17.5,22.8] 0.032 ± 0.011	[22.8,29.8] 0.011 ± 0.004	[5.4,7] 0.57 ± 0.21

Table 3: Modulation amplitudes, for all columns except that labelled CoGeNT the units are counts/day/kg/keVnr, in the CoGeNT column the units are counts/day/kg/keVee, for four bins assuming a best fit overall phase of 106 days, the equivalent energy ranges and rates for other targets, assuming $m_\chi = 7$ GeV and spin-independent scattering cross sections proportional to A^2 . Note that we have not included detector efficiencies or mass fractions in any of the predicted rates.

to A^2 . (Note that we have not included detector efficiencies or mass fractions in any of the predicted rates.)

Let us begin by considering scattering on Si, at CDMS-Si. The modulation above 1.5 keVee should easily appear above threshold at CDMS-Si. Using the results from [46], with 88 kg days, and assuming an efficiency of 0.2, the observed modulation rates would map into a minimum of 3.3 ± 1.4 (5.0 ± 1.5) events for a Maxwellian (106 day) phase. CDMS-Si sees no events below 50 keVnr so this predicted rate is borderline, but not excluded. However, we can draw two further conclusions. First, it suggests that any modulated signal should essentially be 100% modulated (i.e., no sizeable constant piece). Second, invoking significant interference between proton and neutron couplings [47, 48] to reconcile CoGeNT with XENON is likely untenable. Taking $f_n = -0.7f_p$ would turn the relative boost between Si and Ge (the ratio of C_T 's) all the way up to 11, putting any observable modulation in the 1.5-3.1 range in serious conflict with the results from CDMS-Si.

Next, one can consider the rate at CRESST-O. Here the signal in the [0.5–1.5] keVee region translates to a range that is largely below the threshold of many of the individual detectors. However, the [1.5-3.1] keVee range should easily appear in their experiment above 15 keVnr in the oxygen band. With 600 kg days of exposure and an efficiency of 80%, we would expect a modulated signal of 8.75 ± 3.77 (13.1 ± 4.0) events. This is consistent with the ~ 30 events in the same energy range observed [49], where no significant modulation has yet been reported.

Comparing to Xenon we note that the energy range for the high-energy modulation is in a range that is relevant for XENON100. In particular, the 1.5 keVee would lie at 3.7 keVnr in Xenon (again, for a 7 GeV WIMP), where the scintillation efficiency has been studied. Taking an exposure of 1450 kg days ($48 \text{ kg} \times 100.9 \text{ days} \times \text{overall efficiency of } 0.3$), we predict 1020 ± 470 (970 ± 510) events from the third bin and 550 ± 470 (1350 ± 490) events

from the fourth bin *before taking into account the S1 cut*.

Both of these bins are below the S1 threshold for XENON100, of 4 photo-electrons (PE) so we must calculate the probability that an upward fluctuation would occur. Both these bins occur above 3 keVnr, for which results are available for L_{eff} . Taking a value of $L_{eff} = 0.07$ (approximately the lower boundary as measured by [50]), we predict efficiencies of 0.015 and 0.05 for the third and fourth bins, respectively. Thus, with these efficiencies, one would have expected 15.4 ± 7 (14.7 ± 7.7) and 27.4 ± 23.3 (66.9 ± 24.3) events based on the modulation in the third and fourth bins, respectively. To reduce these Poisson efficiencies to an acceptable level would require $L_{eff} \lesssim 0.05$ and $\lesssim 0.04$ for the third and fourth bin, respectively, which lower the rates by a factor of approximately 3 and 6 respectively.

4.3.1 DAMA

Finally, we can consider the signal at the DAMA experiment, and directly compare modulation. For a quenching factor of $Q_{Na} = 0.3$ and $m_\chi \sim 7$ GeV the range in which the CoGeNT modulation is observed roughly corresponds to the range in which the DAMA modulation is observed (see tables 2,3). The *total* modulation observed in the CoGeNT range 0.5-3.1 keVee would yield a modulated rate of 0.04 ± 0.017 cpd/kg (0.065 ± 0.018) for a Maxwellian (best-fit-106 day) phase, which compares with 0.0444 ± 0.0052 cpd/kg (for both MW and best-fit 146 day phases), assuming a conventional spin-independent mapping. Thus, the overall rate at CoGeNT and DAMA seem roughly consistent. In general, however, some of the energy range at CoGeNT will fall above or below the DAMA energy range, meaning that the predicted rate at DAMA from CoGeNT would be somewhat smaller than what is observed. Note that *this is independent of astrophysical model*. As has been noted previously [47, 48], taking the proton and neutron SI couplings to interfere can favor light targets, and correct this. Such effects can happen through interactions via heavy fermionic mediators [48] or through Z 's [51]. However, taking $f_n = -0.7f_p$ (to maximize the suppression at XENON) boosts the modulation at DAMA relative to CoGeNT by a factor of six relative to the case of $f_n = f_p$, which seems in conflict with the data in hand.

We can also consider the specific scenario of [35], with a 7 GeV WIMP and a large quench factor in sodium, $Q_{Na} = 0.5$, [35]. In such a case, the lowest two bins of CoGeNT map roughly into the DAMA range 2-6 keVee, yielding 0.019 ± 0.015 (0.036 ± 0.016) cpd/kg for a Maxwellian (106 day) phase. This is again roughly consistent with DAMA. However, the higher energy bins (1.5-3.1 keVee) map into the range of 6.6-12.7 keVee at DAMA, and predict a modulation of 0.02 ± 0.0085 (0.03 ± 0.009) cpd/kg to be compared with the observed -0.0008 ± 0.0064 cpd/kg observed in the 6-14 keVee range at DAMA, see figure 14. Consequently, this mass and quenching factor would appear in tension with the high energy data. While this conflict is at the 2 (2.7) σ level for Maxwellian (106 day) phase, ignoring it requires one to essentially ignore modulation which is as significant as the modulation that one is taking seriously. As a result, we believe that this particular scenario does not give a good fit to the data.

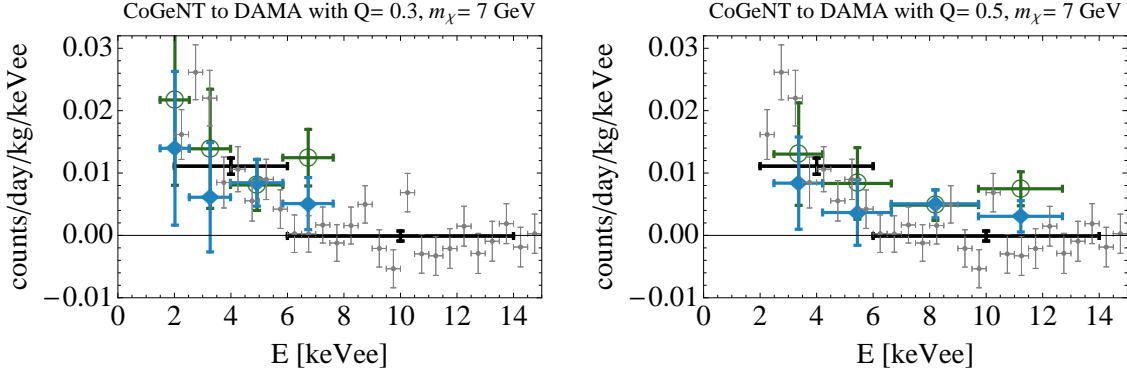


Figure 14: Astrophysics independent comparison of CoGeNT and DAMA modulation amplitudes.

4.3.2 Summary of Halo-Independent Comparisons

A direct comparison of the modulated amplitude allows us to make interesting comparisons between different experiments. The most direct, to CDMS-Ge, shows that the modulation is compatible with CDMS, but only if the modulation is nearly 100%. As a consequence, the modulation should be easily apparent in the CDMS data.

Ultimately, while there is a rough agreement between the size of the CoGeNT modulation and the DAMA modulation, the energy range over which the modulation is spread seems in conflict with previous interpretations [35] invoking a high Q_{Na} , without disregarding a modulation in an energy range which is statistically as significant as in the lower energy range.

Indeed, as expected, the presence of modulation in the high energy range brings about the greatest tensions overall. The absence of a signal at CDMS-Si requires the signal to be highly modulated, while XENON100 should have seen a signal unless L_{eff} is significantly smaller than the measurements of [50].

Such comparisons are only in the context of SI scattering proportional to A^2 . Invoking interference between protons and neutrons to alleviate XENON100 constraints would exacerbate tensions with CDMS-Si, and likely cannot address these questions. Other models, such as SD couplings or iDM would fall outside this analysis, however.

Clearly, if the modulation in the high energy regime persists, any interpretation in terms of spin-independent elastic scattering will be challenging.

5. Conclusions

The search for dark matter is a central element of modern astrophysics, modern cosmology and particle physics. The discovery of particle dark matter is of such importance that any claim must be corroborated by another experiment, and within a single experiment, before it can be believed. The presence of modulation of events in the CoGeNT experiment makes

the possibility of a WIMP signal more compelling, but also requires a serious and thorough discussion, as well as a comparison with predictions from dark matter models.

We have studied the event rate from the CoGeNT experiment over the first 458 days of running. We confirm the original findings of [2] that there appears to be a modulation in the low-energy (0.5-3.1 keVee) data of CoGeNT, with a significance of 99% or 2.6σ (99.7% or 3σ) for a Maxwell-Boltzmann (best fit) phase.

However, the details of the modulation make it somewhat confusing. The significance for modulation in the low energy range (0.5-1.5 keVee), where the signal from a light WIMP would be present, is only 87% (90%) for a Maxwell-Boltzmann (best fit) phase. In contrast, in the higher energy range (1.5-3.1 keVee) the significance is 97.7% (98.3%). The absence of significant modulation in the lower energy range is not, on its own, troubling, because modulation fractions can be higher at higher energies, and cosmogenic backgrounds at 0.9-1.5 keVee are significant. Nonetheless, it is an important point that one cannot claim that the modulation in the low-energy regime gives evidence for a model while simultaneously disregarding the much more significant modulation in the high-energy regime. I.e., if a model does not explain a significant part of the high energy modulation, it cannot be claimed to explain the modulation. The significance of modulation in the 1.5-3.1 keVee region is confirmed by a variety of statistical techniques, and is a significant contributor to the total modulation significance in the 0.5-3.1 keVee energy range.

This result is important, as many DM models with Maxwellian halos will not give any significant modulation in the higher energy range, and often none at all. We have performed a broad study of elastic WIMP scenarios with Maxwellian and NFW-consistent halos. We have found no models that are capable of giving the total modulation and simultaneously producing modulation in the high energy range without having significantly exceeded the *unmodulated* count rate somewhere, although including debris flows [52] or streams might allow it. Our best fit WIMP point with a Maxwell-Boltzmann halo did not significantly improve the fit compared to a constant background. Thus, we believe attempts to understand this modulation with a Maxwellian halo are likely to be unreliable and lead to erroneous conclusions.

To that end, we have attempted to employ techniques that are independent of the halo model [44]. We find that a direct comparison to CDMS-Ge allows the modulation, but predicts a significant modulation should appear at CDMS as well. Note that small errors in energy, while important for interpreting a rapidly falling background, should not affect a general modulation analysis such as this one.

Other conclusions can be drawn from other experiments on the modulation in the 1.5-3.1 keVee range. In particular, the absence of a signal at CDMS-Si suggest that any signal in this range should be $\sim 100\%$ modulated (agreeing with the analysis of CDMS-Ge). A study of XENON100 is intriguing, because the modulation appears in a range that has been more directly calibrated with measurements of Leff. We find that any significant modulation in the 1.5-3.1 range should have shown up at the 10-30+ event level at XENON100, unless the value of L_{eff} is significantly lower than what has been found by [50].

Intriguingly, a halo model-independent comparison to DAMA shows generally *good* agree-

ment between the event rates for a light WIMP and $Q_{Na} \approx 0.3$. We find the modulation at CoGeNT is in conflict with DAMA if one assumes $Q_{Na} = 0.5$, disfavoring previously proposed interpretations utilizing a Maxwellian halo.

Inelastic dark matter models can provide a good fit to the modulation, but not the exponentially falling rate at low energies. iDM in the presence of stream(s) or debris flows could lead to precisely the highly-modulated signal observed. If the signal is only present in April, it could explain why XENON100 did not observe a significant rate, as data taking in that period was limited by excess noise.

In summary, the modulation at CoGeNT is an intriguing piece of the puzzle, but raises as many questions (through the high-energy modulation) as it answers. Future data from CoGeNT illuminating the presence of absence of modulation in both the low and high ranges should clarify whether a - and what kind of - WIMP could give rise to it.

Acknowledgements We are especially grateful to Juan Collar for making the CoGeNT data publicly available and for his support in explaining many aspects of it during our analysis. We also wish to thank Rouven Essig, Roni Harnik, Graham Kribs, Rafael Lang, Josh Ruderman, Tracy Slatyer, Natalia Toro, Michael Witherell and Itay Yavin for useful discussions. ML acknowledges support from the Simons Postdoctoral Fellowship and the LHC Theory Initiative. This research was supported in part by the National Science Foundation under Grant No. NSF PHY05-51164. Fermilab is operated by Fermi Research Alliance, LLC, under Contract DE-AC02-07CH11359 with the United States Department of Energy.

A. CoGeNT data and background

The known background in the energy region of interest arises from cosmogenic electron capture events, which can be modeled as a sum of decaying gaussians. A radioactive element, with Gaussian peak at E_0 , width σ , and half-life $t_{1/2}$ has an energy spectrum of

$$f_{\text{peaks}}(E, t) = N_{\text{atoms}} \frac{\log 2}{t_{1/2}} 2^{-t/t_{1/2}} \frac{1}{\sqrt{2\pi}\sigma} e^{-(E-E_0)/2\sigma^2} . \quad (\text{A.1})$$

Here, N_{atoms} is the total number of atoms expected to decay in the detector. The number of K-shell decays is obtained by fitting to the peaks in the high energy spectrum. These numbers are provided in the public release of the CoGeNT data and are summarized in Table A, where they have been corrected for efficiencies. We have been able to reproduce N_{atoms} for the Ge^{68} peak at 10.4 keVee using our own fitting procedure. The binding energies for the K-shell peaks are given in [1] and the resolution is given by the formula in [53], with parameters from [1].

The expected number of L-shell decays at lower energies is related to the number of K-shell decays [54]; therefore, the second column in Table A can be obtained from the measured quantities in the sixth column. The L-shell cosmogenics are relevant from ~ 0.5 -1.7 keVee,

where the dark matter signal is expected to dominate. The dominant contribution in the first year of running comes from Ge⁶⁸, followed by Zn⁶⁵.

The observed energy spectrum at CoGeNT is affected by an efficiency that captures the decreasing sensitivity to signal near the experiment’s energy threshold. The efficiency is approximately flat at ~ 0.87 between 0.7 - 3.0 keVee, and then drops to 0.75 by 0.5 keVee. Above 4 keVee, it is 0.94. In this work, a spline interpolation of the efficiency data points is used, denoted by $f_{\text{eff}}(E)$.

The CoGeNT data run spanned 458 days, of which 442 were live. The time gaps in which no data were taken must be properly accounted for in a study of annual modulation. To account for these outages, the following function is introduced:

$$f_{\text{gaps}}(t) = (\Theta(67 - t) + \Theta(t - 74)) (\Theta(101 - t) + \Theta(t - 107)) (\Theta(305 - t) + \Theta(t - 308)) , \quad (\text{A.2})$$

where t is measured in days. Therefore, the complete expression for the spectrum of cosmogenic peaks is

$$f_{\text{cosmo}}(E, t) = f_{\text{peaks}}(E, t) f_{\text{gaps}}(t) f_{\text{eff}}(E). \quad (\text{A.3})$$

References

- [1] CoGeNT Collaboration, C. Aalseth *et al.*, Phys.Rev.Lett. **106**, 131301 (2011), 1002.4703.
- [2] CoGeNT Collaboration, C. Aalseth *et al.*, (2011), 1106.0650.

Isotope	$t_{1/2}$ (days)	L-shell			K-shell		
		N_{atoms}	E_0 (keVee)	σ (keVee)	N_{atoms}	E_0 (keVee)	σ (keVee)
As ⁷³	80	14.7	1.41	0.0777	133	11.1	0.120
Ge ⁶⁸	271	736	1.30	0.0770	6460	10.4	0.117
Ga ⁶⁸	271	60.9	1.19	0.0764	553	9.66	0.114
Zn ⁶⁵	244	243	1.10	0.0759	2250	8.98	0.112
Ni ⁵⁶	5.9	1.78	0.926	0.0749	17.2	7.71	0.107
Co ^{56,58}	71	10.9	0.846	0.0744	107	7.11	0.104
Co ⁵⁷	271	2.98	0.846	0.0744	29.3	7.11	0.104
Fe ⁵⁵	996	51.8	0.769	0.0740	489	6.54	0.102
Mn ⁵⁴	312	24.3	0.695	0.0736	238	5.99	0.100
Cr ⁵¹	28	3.38	0.628	0.0732	33.5	5.46	0.0975
V ⁴⁹	330	17.2	0.564	0.0728	172	4.97	0.0953

Figure 15: Data used to model the cosmogenic background for both L-shell and K-shell decays. N_{atoms} is the number of atoms in the detector expected to decay via each mode (before efficiency corrections), E_0 is the binding energy in keVee, σ is the energy resolution in keVee, and $t_{1/2}$ is the half-life for the decay in days.

- [3] D. Hooper and C. Kelso, (2011), 1106.1066.
- [4] A. Drukier, K. Freese, and D. Spergel, *Phys.Rev.* **D33**, 3495 (1986).
- [5] J. Lewin and P. Smith, *Astropart.Phys.* **6**, 87 (1996).
- [6] R. Gaitskell, *Ann.Rev.Nucl.Part.Sci.* **54**, 315 (2004).
- [7] DAMA Collaboration, R. Bernabei *et al.*, *Eur.Phys.J.* **C56**, 333 (2008), 0804.2741.
- [8] R. Bernabei *et al.*, *Eur.Phys.J.* **C67**, 39 (2010), 1002.1028.
- [9] XENON100 Collaboration, E. Aprile *et al.*, *Phys.Rev.Lett.* (2011), 1104.2549.
- [10] XENON10 Collaboration, J. Angle *et al.*, *Phys.Rev.Lett.* **100**, 021303 (2008), 0706.0039.
- [11] XENON10 Collaboration, J. Angle *et al.*, (2011), 1104.3088.
- [12] M. Felizardo *et al.*, *Phys.Rev.Lett.* **105**, 211301 (2010), 1003.2987.
- [13] M. Felizardo *et al.*, (2011), 1106.3014.
- [14] CDMS-II Collaboration, Z. Ahmed *et al.*, *Science* **327**, 1619 (2010), 0912.3592.
- [15] CDMS-II, Z. Ahmed *et al.*, *Phys. Rev. Lett.* **106**, 131302 (2011), 1011.2482.
- [16] J. Collar, (2011), 1106.0653.
- [17] J. Collar, (2010), 1010.5187.
- [18] J. Collar, (2010), 1006.2031.
- [19] J. Collar and D. McKinsey, (2010), 1005.3723.
- [20] J. Collar and D. McKinsey, (2010), 1005.0838.
- [21] J. Collar, (2011), 1103.3481.
- [22] J. Collar, Private communication, 2011.
- [23] M. T. Frandsen *et al.*, (2011), 1105.3734.
- [24] T. Schwetz and J. Zupan, (2011), 1106.6241.
- [25] G. Cowan, *Phys. Lett. B* **667**, 320 (2008).
- [26] J. D. Scargle, *Astrophys. J.* **263**, 835 (1982).
- [27] N. R. Lomb, *Astrophysics and Space Science* **39**, 447 (1976).
- [28] SNO Collaboration, B. Aharmim *et al.*, *Phys.Rev.* **D72**, 052010 (2005), hep-ex/0507079.
- [29] W. H. Press, B. P. Flannery, S. A. Teukolsky, and W. T. Vetterlin, *Numerical Recipes in C* (Cambridge University Press, 1988).
- [30] P. Belli *et al.*, (2011), 1106.4667.
- [31] J. Kopp, T. Schwetz, and J. Zupan, *JCAP* **1002**, 014 (2010), 0912.4264.
- [32] R. Bernabei *et al.*, *Eur. Phys. J.* **C53**, 205 (2008), 0710.0288.
- [33] N. Bozorgnia, G. B. Gelmini, and P. Gondolo, (2010), 1006.3110.
- [34] R. Bernabei *et al.*, *Phys. Lett.* **B389**, 757 (1996).

- [35] D. Hooper, J. Collar, J. Hall, and D. McKinsey, *Phys.Rev.* **D82**, 123509 (2010), 1007.1005.
- [36] C. McCabe, (2010), 1005.0579.
- [37] M. Lisanti, L. E. Strigari, J. G. Wacker, and R. H. Wechsler, *Phys.Rev.* **D83**, 023519 (2011), 1010.4300.
- [38] D. Tucker-Smith and N. Weiner, *Phys.Rev.* **D64**, 043502 (2001), hep-ph/0101138.
- [39] R. F. Lang and N. Weiner, *JCAP* **1006**, 032 (2010), 1003.3664.
- [40] M. C. Smith *et al.*, *Mon.Not.Roy.Astron.Soc.* **379**, 755 (2007), astro-ph/0611671.
- [41] J. Bovy, D. W. Hogg, and H.-W. Rix, *Astrophys.J.* **704**, 1704 (2009), 0907.5423.
- [42] P. J. McMillan and J. J. Binney, (2009), 0907.4685.
- [43] M. Reid *et al.*, *Astrophys.J.* **700**, 137 (2009), 0902.3913.
- [44] P. J. Fox, J. Liu, and N. Weiner, *Phys. Rev.* **D83**, 103514 (2011), 1011.1915.
- [45] P. J. Fox, G. D. Kribs, and T. M. Tait, *Phys.Rev.* **D83**, 034007 (2011), 1011.1910.
- [46] CDMS, J. Filippini, *Nuovo Cim.* **C32N5-6**, 45 (2009).
- [47] S. Chang, J. Liu, A. Pierce, N. Weiner, and I. Yavin, *JCAP* **1008**, 018 (2010), 1004.0697.
- [48] J. L. Feng, J. Kumar, D. Marfatia, and D. Sanford, (2011), 1102.4331.
- [49] F. Proebst, (Nov, 2010).
- [50] G. Plante *et al.*, (2011), 1104.2587.
- [51] P. J. Fox, J. Liu, D. Tucker-Smith, and N. Weiner, (2011), 1104.4127.
- [52] M. Lisanti and D. N. Spergel, (2011), 1105.4166.
- [53] CoGeNT Collaboration, C. Aalseth *et al.*, *Phys.Rev.Lett.* **101**, 251301 (2008), 0807.0879, Erratum: *Phys.Rev.Lett* 102, 109903(E) (2009).
- [54] J. N. Bahcall, *Phys.Rev.* **132**, 362 (1963).